REPORT

Dynamic functional connectivity assesses the progression of Parkinson's disease

Zhibao Li,[1,2] Wei Chen,[1] Xiaoyu Zeng,[4] Jun Ni,[4] Yuzhu Guo,[5] Hua Zhang,[1] Yang Li,[5,*] Yina Ma,[4,6,*] and Fangang Meng[2,3,6,*]

*Correspondence: liyang@buaa.edu.cn (Y.L.); yma@bnu.edu.cn (Y.M.); mengfg@ccmu.edu.cn (F.M.)

Received: July 9, 2023; Accepted: September 9, 2023; Published Online: September 11, 2023; https://doi.org/10.59717/j.xinn-med.2023.100027

GRAPHICAL ABSTRACT

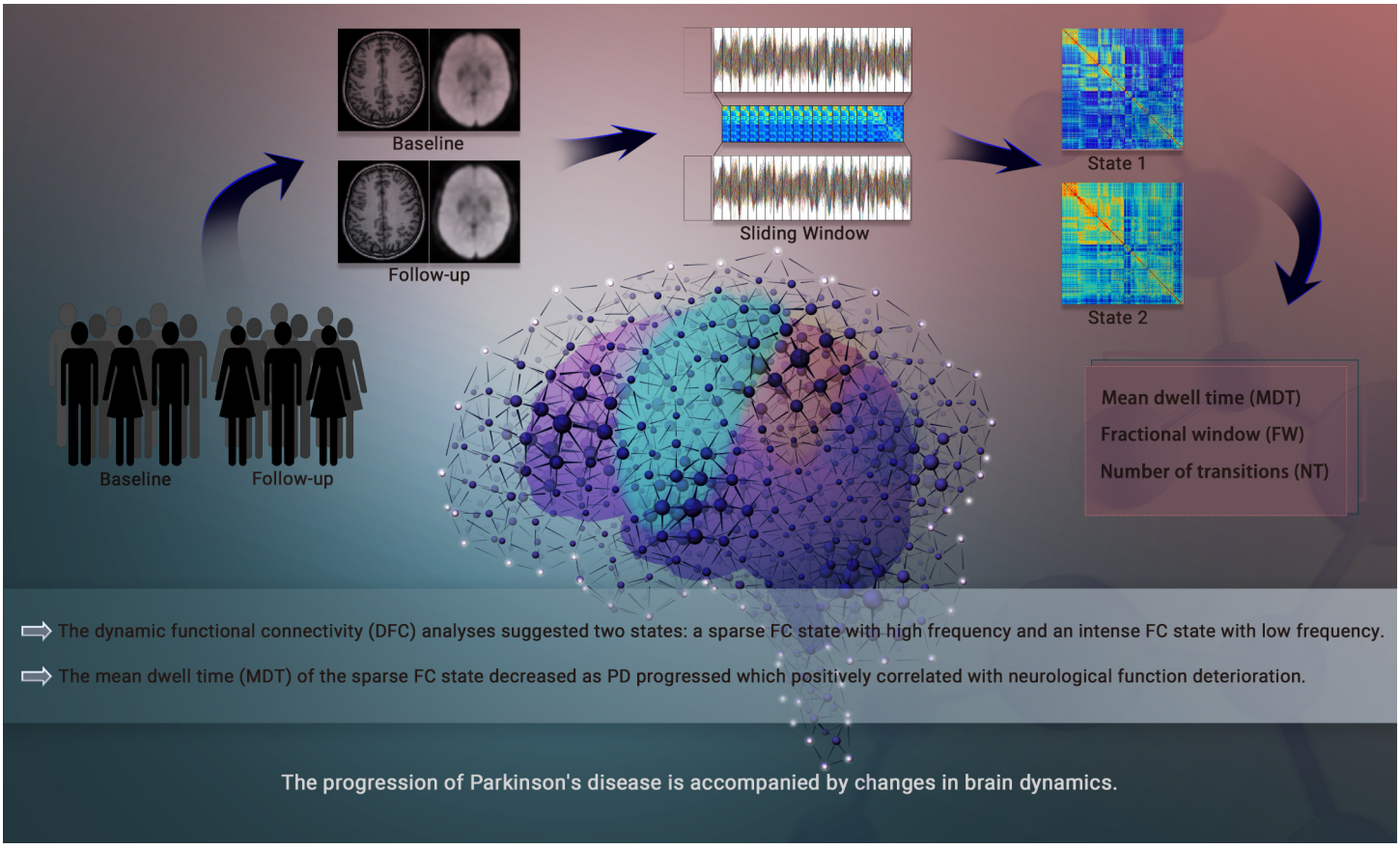

PUBLIC SUMMARY

- Progression of Parkinson's disease (PD) induces modulations in dynamic functional brain networks.
- Changes of dynamics functional brain network are linked to worsening PD symptoms.
- Dynamic brain network has potential as a biomarker for evaluating PD progression.

REPORT

www.the-innovation.org/medicine

Dynamic functional connectivity assesses the progression of Parkinson's disease

Zhibao Li,[1,2] Wei Chen,[1] Xiaoyu Zeng,[4] Jun Ni,[4] Yuzhu Guo,[5] Hua Zhang,[1] Yang Li,[5,*] Yina Ma,[4,6,*] and Fangang Meng[2,3,6,*]

[1]Department of Neurosurgery, The First Affiliated Hospital of Xi'an Jiaotong University, Xi'an 710061, China
[2]Department of Neurosurgery, Beijing Neurosurgical Institute, Capital Medical University, Beijing 100070, China
[3]Department of Functional Neurosurgery, Beijing Tiantan Hospital, Capital Medical University, Beijing 100070, China
[4]State Key Laboratory of Cognitive Neuroscience and Learning, IDG/McGovern Institute for Brain Research, Beijing Normal University, Beijing 100875, China
[5]Department of Automation Sciences and Electrical Engineering, Beihang University, Beijing 100191, China
[6]Chinese Institute for Brain Research, Beijing 102206, China
*Correspondence: liyang@buaa.edu.cn (Y.L.); yma@bnu.edu.cn (Y.M.); mengfg@ccmu.edu.cn (F.M.)

Received: July 9, 2023; Accepted: September 9, 2023; Published Online: September 11, 2023; https://doi.org/10.59717/j.xinn-med.2023.100027

Citation: Li Z., Chen W., Zeng X., et al., (2023). Dynamic functional connectivity assesses the progression of Parkinson's disease. The Innovation Medicine **1(2)**, 100027.

Parkinson's disease (PD) induces functional connectivity (FC) changes during its course. However, the impact of PD progression on the temporal properties of FC remains ambiguous. In the current study, we aimed to uncover longitudinal shifts in dynamic FC (DFC) temporal properties of brain networks during PD progression, proposing a novel biomarker for PD progression evaluation. We conducted a longitudinal study on 45 PD patients from the Parkinson's Progression Markers Initiative database. Patients underwent dual-timepoint neurological assessments and resting-state fMRI scans at baseline and 1-4 years of subsequent follow-up. The sliding-window technique and k-means clustering were employed to scrutinize DFC patterns of the entire brain network, including individual cortical subnetworks and subcortical nuclei (SN) at every timepoint. From this analysis, DFC analyses revealed two predominant states: a high-frequency sparse FC state and a low-frequency intense FC state. For the entire brain network, the mean dwell time (MDT) in the sparse FC state diminished with PD progression, and this decrease was closely tied to motor deterioration. Concerning cortical subnetworks and SN, MDTs in the sparse FC state reduced at the second timepoint in both visual (VN) and limbic networks (LN) linked with the SN. The MDT reduction in LN-SN positively correlated with cognitive decline, while the MDT reduction in VN-SN showed a strong link with motor degradation. These results emphasize that DFC might offer insights into the evolving brain dynamics in PD patients over the disease's course, underscoring its prospective utility as a progression biomarker.

INTRODUCTION

Parkinson's disease (PD) ranks as the second-most prevalent neurodegenerative disorder.[25] Its primary etiology stems from dopamine neurotransmission deficits due to dopaminergic neuron degeneration in the substantia nigra, leading to a spectrum of motor and non-motor symptoms.[29] As the disease evolves, these symptoms intensify, profoundly compromising patient well-being and safety. Gaining deeper insights into PD progression is pivotal for the timely introduction of therapeutic interventions, subsequently enhancing patients' life quality. However, there's a pressing need for dependable biomarkers that can effectively trace PD progression.

Resting-state (RS) functional connectivity (FC) MRI presents an invaluable tool to gauge the brain's functional network status without the potential biases of task performance. Earlier studies have illuminated its potential in delineating disease progression trajectories.[5,11,20,23] A study by Filippi M et al. showcased that longitudinal whole-brain FC variations differ among PD patients at various disease stages, observing a mix of hypo- and hyper-connectivity linked with symptomatic developments.[11] This suggests that PD progression indeed instigates notable changes in the functional brain network, emphasizing a relationship between disease evolution and these functional shifts. Nevertheless, a majority of prior works overlooked the potential influence of PD progression on the patient's dynamic functional connectivity (DFC) and its capability to monitor PD evolution.

Contrary to static FC, DFC encapsulates functional connectivity dynamics, often viewed as a more precise portrayal of neural networks. Preliminary cross-sectional analyses have highlighted significant deviations in the temporal facets of specific FC patterns in PD patients' DFC compared to healthy counterparts, both globally[12,18] and within the interplay between cortical and subcortical networks.[7] Yet, the question remains: how does PD progression reshape the temporal dynamics and patterns of DFC? To unravel this, we utilized dual-timepoint clinical and RS-fMRI datasets at baseline and during a 1-4 year follow-up to probe DFC's longitudinal shifts with PD evolution, utilizing a sliding windows strategy. This analysis encompassed the entire brain network and interactions between cortical subnetworks and the subcortical nucleus (SN), aiming to discern connections with clinical symptom amplification.

This study aimed to (1) Detect longitudinal shifts in DFC temporal properties across global brain networks during PD progression. (2) Unearth longitudinal transformations in DFC temporal properties within specific subnetwork partitions[27] and SN amidst PD progression. (3) Associate these temporal properties changes with neurological function deterioration, aspiring to establish a groundbreaking biomarker for PD progression assessment.

MATERIALS AND METHODS

Data source

Participants' data were sourced from the Parkinson Progression Markers Initiative (PPMI) database (http://www.ppmi-info.org). Local research ethics committees approved all PPMI-affiliated studies. Prior to the study's commencement, every participant furnished written informed consent. This research incorporated only those patients who had available imaging (comprising fMRI and structural scans) and clinical assessment data. A total of 72 PD patients, who were subjected to dual-timepoint imaging and clinical evaluations at baseline and subsequent follow-up between 1 and 4 years, were included. Figure 1 delineates the process of data selection, processing, and analysis.

Clinical assessments

The PPMI dataset facilitated comprehensive motor and non-motor neurological evaluations of the patients. For a thorough longitudinal examination, we selected specific assessment scales, ensuring that they were implemented at both the evaluated timepoints. Daily non-motor and motor experiences were gauged using the Movement Disorder Society Unified Parkinson's Disease Rating Scale part I (UPDRS-I) and part II (UPDRS-II). The UPDRS-III and IV scales determined PD's motor signs and complications. Sleep disturbances were quantified via the Epworth Sleepiness Scale (ESS) and the Rapid Eye Movement Sleep Behavior Disorder Screening Questionnaire (RBDSQ), while the Montreal Cognitive Assessment (MoCA) evaluated cognitive impairments.

Image acquisition and preprocessing

To maintain result consistency and reliability, identical scanning parameters were used for imaging data at both timepoints. A 3.0-Tesla SIEMENS Prisma scanner was employed for image acquisition. Structural images were acquired using three-dimensional T1-weighted MPRAGE with flip angle (FA) = 90°, matrix X = 256 pixels, matrix Y = 256 pixels, matrix Z = 176, pixel spacing X = 1 mm, pixel spacing Y = 1 mm, slice thickness = 1.2 mm, echo time (TE) = 2.9 ms, and repetition time (TR) = 2300 ms. RS-fMRI data were acquired using an echo-planar imaging sequence that lasted 7 min (210 volumes) with

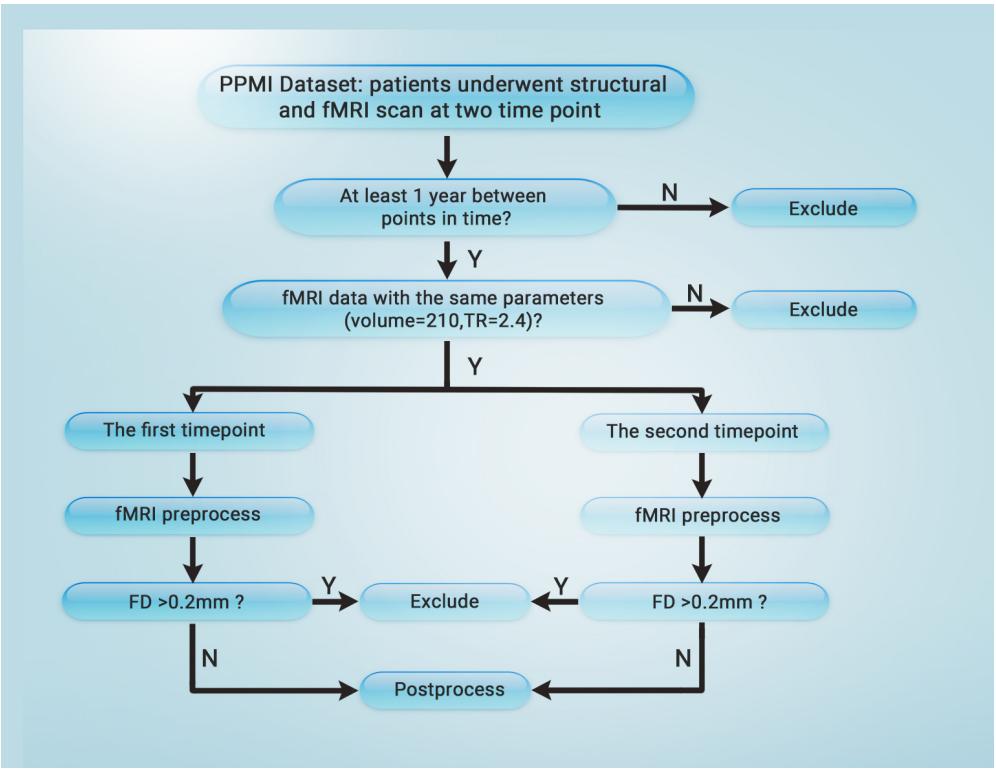

Figure 1. The flowchart to provide an overview of the data screening, processing, and analysis procedures.

TR = 2400 ms, TE = 25 ms, FA = 80°, matrix X = 518 pixels, matrix Y = 518 pixels, pixel spacing X = 3 mm, pixel spacing Y = 3 mm, and slice thickness = 3 mm.

DPABISurf, a derivative of the DPABI/DPARSF toolbox designed for surface-based RS-fMRI data analysis, was employed for image data preprocessing,[6,34] with the fMRIprep pipeline overseeing the structural and functional MRI data processing.[10] An exhaustive six-step process was utilized for MRI data processing, further elaborated upon in the supplemental information section.

Extract time courses for regions of interest

We used numerous cortical regions and SN as regions of interest (ROI). Cortical regions were mapped using the Schaefer 200 ROI cortical brain atlas.[27] The 200 ROIs belong to seven brain networks, namely visual network (VN), sensorimotor network (SMN), dorsal attention network (DAN), ventral attention network (VAN), limbic network (LN), frontoparietal network (FTN), and default mode network (DMN). The SN were defined using the Tian 16 ROI subcortical brain atlas.[31] The time series of the 216 ROIs were extracted. To avoid the effect of brain parcellations on the results, the cortical regions were also defined by the Schaefer 400 ROI cortical brain atlas[27] and the Tian 16 ROI subcortical brain atlas.

Quality control for head motion

Prior to initiating the DFC analysis, a rigorous head motion quality check was undertaken. Any patient demonstrating a mean framewise displacement (FD) surpassing 0.2 mm was excluded from successive evaluations. A finalized cohort of 45 patients was established for subsequent analyses post exclusions.

DFC analysis of the whole brain network

Sliding window approach. The DFC analysis was conducted using a sliding window approach and the k-means cluster algorithm in the DynamicBC toolbox(version 2.2, http://www.restfmri.net/forum/DynamicBC).[21] Based on prior research,[1] we chose a 44-second window spanning 22 volumes, convolved with a 3 TR Gaussian kernel. This window moved in single TR increments across 200 volumes, resulting in 179 overlapping windows with a 96% overlap. Within this framework, Pearson linear correlation coefficients were calculated between ROI pairs, producing FC maps with 216 x 216 covariance matrices for each participant. To normalize these maps, we applied Fisher's z transformation, yielding 179 dynamic FC maps per participant to represent DFC variations during scanning. For added robustness, we also employed the flexible least squares (FLS) method to generate a DFC map for every scan timepoint. Further details on the FLS approach can be found in the Supplementary Materials asd Methods.

Clustering analysis. Based on prior research,[1] we applied the k-means clustering algorithm to discern recurring FC maps, or "states", gauged by their frequency and structure. By amalgamating all FC maps across subjects from both timepoints, a collective FC map of 16,110 windows was produced. To gauge the similarity between these FC maps, we employed the L1 Manhattan distance-effective for high-dimensional data. To ascertain the optimal cluster count, three criteria were utilized: Calinski-Harabasz (CH), Davies-Bouldin (DB), and silhouette indices. The final optimal number of clusters was obtained by averaging the values obtained from the above three algorithms and rounding up. The optimal cluster number was determined by varying k from 2 to 10.

For the temporal dynamics of DFC, we examined mean dwell time (MDT), fractional window (FW), and number of transitions (NT). MDT gauges average continuity within the same state; FW signifies the ratio of windows in a specific state; and NT encapsulates state transitions for each participant. Variations in MDT, FW, and NT across PD patient timepoints were analyzed using paired t-tests ($p < 0.05$, FDR corrected).

DFC analysis of cortical subnetworks and SN

We investigated the DFC across the entire brain, encompassing all cortical areas and the SN. Furthermore, we separately analyzed each of the seven cortical subnetworks and the SN. For each subnetwork, we extracted the relevant time series and subsequently merged it with the SN's time series, resulting in seven distinct time series. These were then subjected to DFC analysis using the sliding window approach and k-means clustering algorithm, maintaining consistent parameters as established earlier. We then contrasted the temporal properties of states across two observation points.

Relationship between neurological functions and temporal properties

To ascertain the link between the decline in neurological function and the longitudinal shifts in temporal properties, we executed a correlation analysis, juxtaposing the z-scored difference in neurological assessments with the z-scored difference in temporal properties. This analytical approach was employed in the DFC evaluation of the entire brain network, as well as in the examination of cortical subnetworks in conjunction with SN. A p-value of less than 0.05 was deemed statistically significant.

RESULTS

Demographic and clinical characteristics

In the final analysis, our cohort comprised 45 patients. We had to exclude 27 patients owing to excessive head movement, quantified as a FD greater than 0.2 mm. Both DFC data and clinical neurological evaluations were ascertained at two distinct timepoints for every participant, adhering to a within-subjects design paradigm. Table 1 delineates the comprehensive demographic and clinical profile of the participants.

DFC state analysis

Clustering analysis and the DFC states. Using optimal clustering criteria,

Table 1. The demographic and clinical characteristics of participants

	Stage 1	Stage 2	P-value
Sex	14 F, 31 M	14 F, 31 M	-
Age	58.7 (10.3)	61.5 (10.2)	P<0.001
UPDRS-I	4.1 (3.0)	6.2 (3.9)	P<0.001
UPDRS-II	5.4 (3.5)	7.9 (4.3)	P<0.001
UPDRS-III	18.9 (9.2)	25.3 (11.1)	P<0.001
UPDRS-IV	0.4 (1.4)	1.2 (2.6)	P=0.01
ESS	8.1 (4.3)	11.1 (4.8)	P<0.001
RBDSQ	5.4 (2.6)	6.2 (3.2)	P=0.026
MoCA	27.9 (2.7)	27.2 (2.6)	P=0.007

we discerned two distinct FC states, both consistently observed across individual scans and the patient cohort (Supplementary Figure 1). State I was characterized by sparse connectivity among brain regions, robust connections in specific between-networks (notably VN-DAN, SMN-DAN, SMN-VAN), and within networks like VN, SMN, and VAN. It manifested prominently, observed 9,881 times, and constituted 61.33% of all states (Figure 2A). In contrast, State II showcased broader, stronger inter-regional connections but was less recurrent, with 6,229 instances, representing 38.67% of all occurrences (Figure 2A). Notably, the prevalence of State I was statistically more significant than that of State II, with percentages of 61.33%±29.19% vs. 38.67%±29.19% ($p<0.01$).

Figure 3A and 3B show timepoint-specific FC states obtained using the k-means clustering analysis and the top 1% connections in each state, respectively. Similarly, the state I exhibited sparse FC between brain regions with strong connections in several between-networks (VN-DAN, SMN-DAN, and SMN-VAN) and within-networks (VN, SMN, and VAN). While state II showed stronger positive FC between brain regions.

Figures 3A and 3B display the timepoint-specific FC states determined through k-means clustering analysis and the dominant 1% of connections within each state, respectively. Analogously, State I demonstrated sparse FC amongst brain regions, coupled with pronounced connections in several between-networks such as VN-DAN, SMN-DAN, and SMN-VAN, and within the VN, SMN, and VAN networks. In contrast, State II was characterized by more intensified positive FC between brain regions.

Temporal properties of FC states in the two timepoints.. We further delved into discerning whether the temporal attributes of FC states exhibited alterations concomitant with the progression of PD. Notably, the FW did not demonstrate significant temporal variations for either State I (0.63±0.30 vs 0.60±0.30, p=0.42; FDR corrected, Figure 4A) or State II (0.37±0.30 vs 0.40±0.30, p=0.42; FDR corrected, Figure 4A). However, a compelling difference was observed in the MDT for State I between the two timepoints. The MDT for State I at timepoint II was significantly truncated compared to timepoint I (58.38±61.06 vs 39.93±44.02, p=0.004; FDR corrected; Figure 4B), implicating a reduction in dwell time for the sparse FC state as PD advanced. Intriguingly, the state transitions' frequency remained consistent across the timepoints (5.51±3.88 vs 6.53±4.05, p=0.13; FDR corrected, Figure 4C). In a subsequent analysis aiming to establish associations between MDT decline and neurological decline, a prominent positive correlation was identified: the diminishing MDT in State I was conjoined with exacerbated motor function decline (r=0.63; p<0.001; Figure 4D). This suggests that the deterioration in motor function is intertwined with a more pronounced decline in State I's MDT.

DFC analysis of cortical subnetworks and SN. To explore the longitudinal alterations in DFC across individual cortical subnetworks and SN in PD patients, we employed a sliding window approach and clustering analysis on the time series data of each subnetwork and SN. Our results revealed a pattern parallel to whole-brain DFC. Specifically, DFC analyses within each subnetwork and SN isolated two salient FC states: a frequently occurring but sparsely connected state and a less common yet more robustly connected

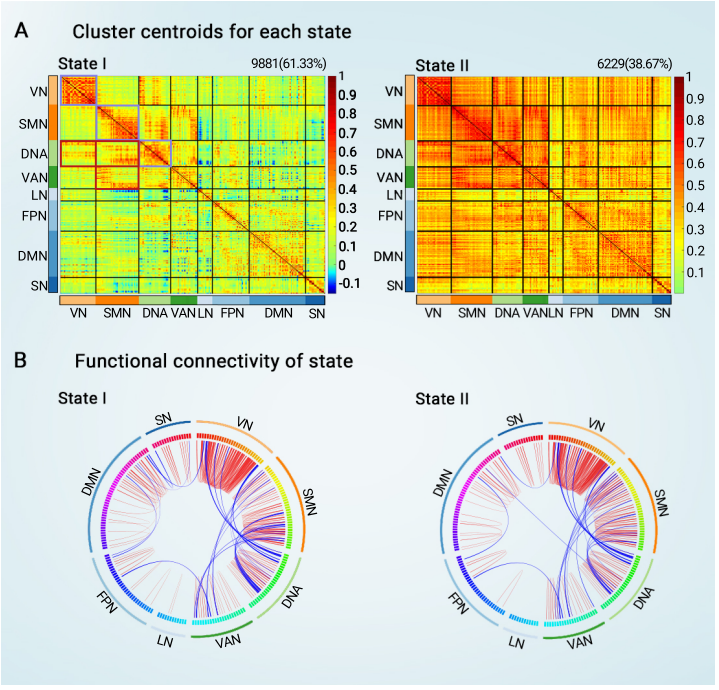

Figure 2. Results of the clustering analysis for each state (A) Cluster centroids for each state. The total number of occurrences and percentage of total occurrences are listed above each cluster median. The blue box indicates strong within-network connections, and the red box indicates strong between-network connections. (B) The chordal graph generated using Circos shows only the top 1% of connections for each state. Red lines represent connections within-network, while blue lines depict connections between-networks. VN = visual network, SMN = sensorimotor network, DAN = dorsal attention network, VAN = ventral attention network, LN = limbic network, FPN = frontoparietal network, DMN = default mode network, SN = subcortical nucleus

state (as evidenced in Figure 5A & 5D). Notably, deviations in temporal DFC properties were evident in LN-SN and VN-SN. In the LN-SN domain, the MDT for the sparse connections (termed State II) exhibited a marked reduction during timepoint II (40.77±47.66 vs. 24.52±16.93; p=0.023, FDR-corrected, Figure 5B). A parallel trend was discerned in VN-SN, with the MDT of sparse connections (State I) also diminishing significantly at timepoint II (36.21±37.96 vs. 23.36±17.61; p=0.023, FDR-corrected, Figure 5E). Further correlational analyses underscored that the MDT decline in LC-SN was associated with cognitive weakening (r=0.46, p=0.001, Figure 5C), and the MDT dip in VN-SN correlated with deteriorating motor function (r=0.72, p<0.001, Figure 5F) among PD patients.

To validate the robustness of our findings across varied ROIs and analytical techniques, we executed a DFC analysis using a sliding window approach for 416 ROIs and the FLS method for 216 ROIs. Consistent with our primary analysis, we observed analogous results (refer to Supplementary Figures 2-7). Specifically, the MDT of sparse FC states at timepoint II was significantly diminished compared to timepoint I. Further, a positive correlation emerged between the extent of MDT reduction in these sparse FC states and the decline in motor function. Comprehensive details of these observations are elaborated upon in the supplemental material. Collectively, these findings underscore the replicability and robustness of our results, suggesting they are not contingent on a specific methodological approach or parcellation scheme.

DISCUSSION

In this investigation, we delved into the longitudinal changes of DFC in PD patients by leveraging two-timepoint imaging alongside clinical neurological evaluations. Echoing findings from prior research,[12,18] we discerned two distinct DFC states: a prevalent state characterized by sparse connections and a less frequent state marked by robust interconnections. Importantly, as PD advanced, the MDT associated with these sparse connections exhibited a pronounced decline. This reduction was positively aligned with the worsening of neurological functions. To bolster the credibility of our outcomes, we employed diverse parameters and methodologies, underscoring the robust-

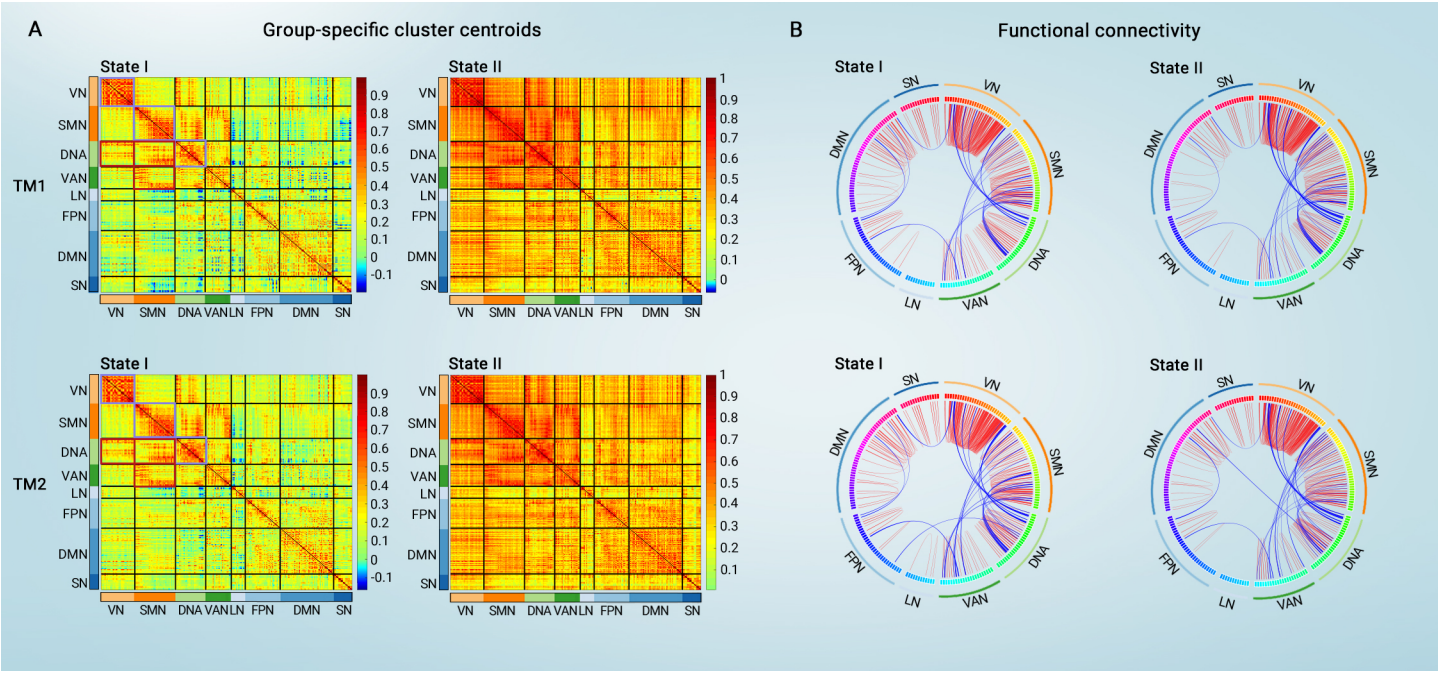

Figure 3. Functional connectivity state results (A) Timepoint-specific cluster centroid for each state. The blue box indicates strong within-network connections, and the red box indicates strong between-network connections. (B) The chordal graph generated using Circos shows only the top 1% of connections for each state for timepoints I and II. Red lines represent connections within-network, while blue lines depict connections between-networks. VN = visual network, SMN = sensorimotor network, DAN = dorsal attention network, VAN = ventral attention network, LN = limbic network, FPN = frontoparietal network, DMN = default mode network, SN = subcortical nucleus, TM1 = timepoint I, TM2 = timepoint II.

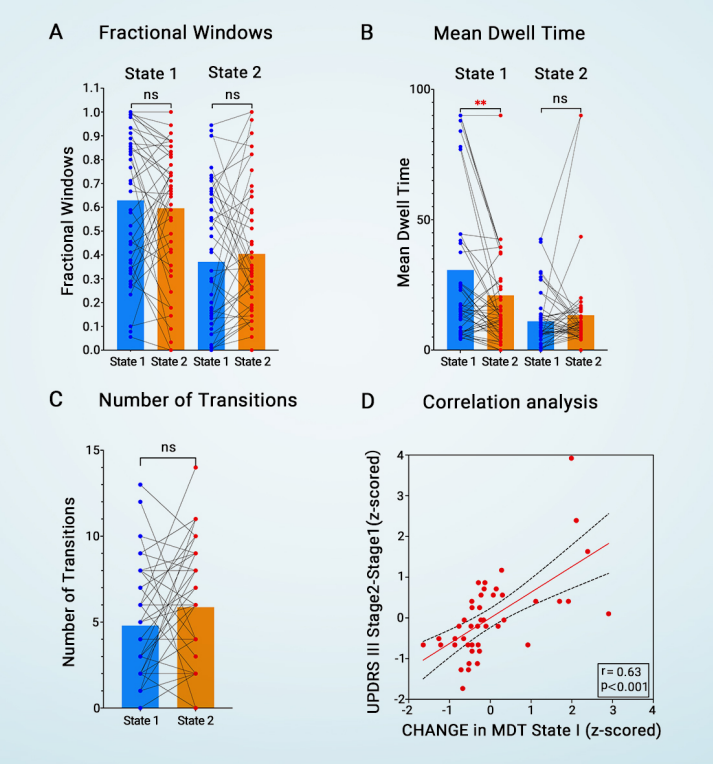

Figure 4. Results of the between-timepoint comparisons of temporal properties of each state (A) Results of the between-timepoint comparisons of fractional windows for each state. (B) Results of the between-timepoint comparisons of mean dwell time for each state. (C) Results of the between-timepoint comparisons of the number of transitions for each state. (D) Results of correlation analysis between MDT changes (z-scored) in state I and motor worsening (z-scored). (**p < 0.01, FDR corrected).

ness and consistency of our findings.

PD is a multifaceted neurodegenerative disorder, rendering predictions regarding its progression challenging. While numerous studies have harnessed sophisticated neuroimaging techniques to pinpoint potential biomarkers for gauging PD progression,[11,20,24] the practical applicability of these markers is still under scrutiny. This limited utility may stem from the constrained dimensions inherent in the neuroimaging data. DFC encompasses both spatial and temporal facets, underscoring the evolving nature of FC rather than a static portrayal, offering a more nuanced representation of functional brain networks.[17] In our current endeavor, we employed DFC to monitor PD's evolution, affirming its potential as a compelling biomarker for assessing PD progression. Specifically, a diminished MDT in sparse connections could be emblematic of PD's advancement. These receding MDTs in sparse connections might hint at a scenario where PD progression adversely impacts the functionality of several between-networks (VN-DAN, SMN-DAN, SMN-VAN) and within-networks (VN, SMN, DAN).

Efficient cognition fundamentally relies on the integrative functions of between-network communication, while motor execution is underpinned by within-network communication.[8] In our findings, a significant association was observed between the MDT decline in state I and motor exacerbation. This may be ascribed to diminished integrative function within the networks of VN, SMN, and DAN. Historically, PD has been linked to dysfunction in the visual network, engendering specific visual perturbations.[16,33] Such disruptions can influence a spectrum of motor and non-motor behaviors, spanning from visuospatial function to the perception of gait functionality.[9,16] Moreover, the cornerstone of PD diagnosis remains motor symptomatology, spurred by malfunctions in the sensorimotor area. Such dysfunctionality prompts FC alterations within the SMN, culminating in hindered sensorimotor integration.[19,30] This is probably rooted in the cortico-striatal pathway's denervation, consequent to the degeneration of nigrostriatal dopaminergic neurons.[15,28] As PD advances, compounded by an escalated loss of these neurons, the FC anomalies within the SMN intensify.[11,20] Furthermore, the DAN is posited to regulate the top-down voluntary attention allocation pivotal for task-specific motor execution.[32] Holistically, an aberrant integrative function within the VN, SMN, and DAN networks correlates with the motor functional decline observed in PD patients – a resonance with prior research outcomes. Although our study detected reduced integrative function in certain between-networks (VN-DAN, SMN-DAN, SMN-VAN) within state I, a direct tie to cognitive function remained elusive, potentially attributable to the nuances of network parcellation. Still, it's crucial to recognize the intimate interplay between DAN, VN, and SMN in modulating PD patients' mobility. A

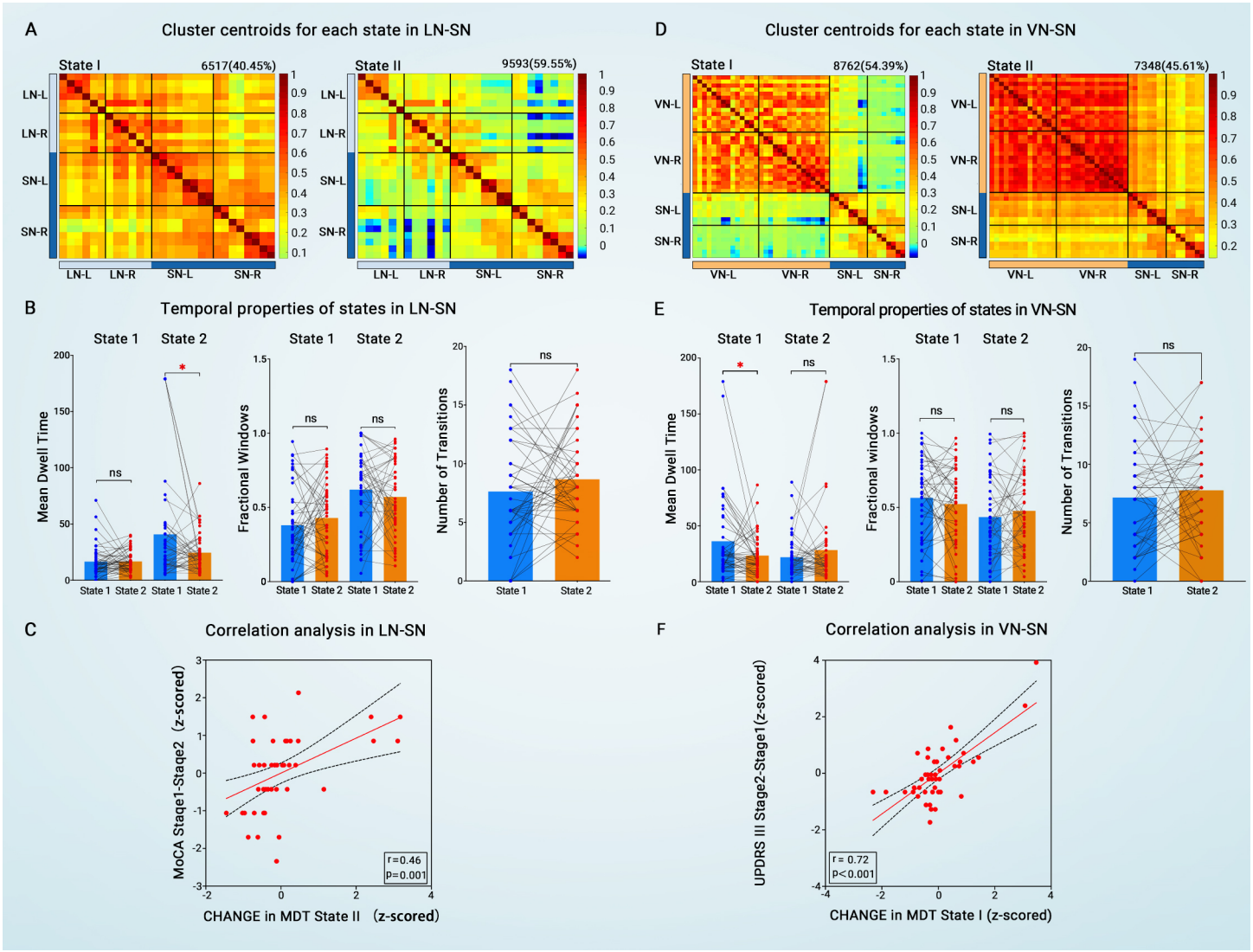

Figure 5. Results of DFC analysis of LN-SN and VN-SN (A) Cluster centroids for each state in DFC analysis of LN-SN. The total number of occurrences and percentage of total occurrences are listed above each cluster median. (B) Between-timepoint comparisons of temporal properties of each state in DFC analysis of LN-SN. (C) Results of correlation analysis between state II MDT changes (z-scored) and cognitive attenuation (z-scored) in DFC analysis of LN-SN. (D) Cluster centroids for each state in VN-SN. (E) Between-timepoint comparisons of temporal properties of each state in DFC analysis of VN-SN. (F) Results of correlation analysis between state I MDT changes (z-scored) and motor worsening (z-scored) in DFC analysis of VN-SN. (*p < 0.05, FDR corrected).

decline in VN-DAN FC might perturb the DAN's regulatory role during visuospatial attention shifts, resulting in aberrant gait patterns in PD patients.[35] Similarly, a reduced FC within SMN-DAN could hamper cognitive strategies pivotal for gait coordination.[35] Collectively, these findings underscore the fluid nature of DFC, both within and across networks, as PD evolves, perpetuating a relentless decline in motor capabilities.

We investigated the longitudinal DFC variations in each of the seven cortical subnetworks and the salience network SN in PD. Altered temporal properties were particularly notable in the LN-SN and VN-SN. The LN, incorporating the orbitofrontal cortex and temporal pole, has regions like the hippocampus vital for cognitive functions. Established neural circuits link the SN with the limbic system, influencing cognitive processes like memory, learning, and emotion.[3,14] Prior research highlights LN–SN pathway dysfunction in PD patients.[4,22] Our findings emphasize the evolving DFC within this pathway, possibly mirroring the progressive cognitive dysfunctions in PD. Similarly, the VN-SN demonstrated a decline in the MDT of sparse FC states, strongly correlating with deteriorating motor function. Impairments within the VN-SN can indirectly cause motor dysfunction due to the pivotal role of the visual pathways in visuospatial construction and motion perception.[33] Moreover, Guan et al.[13] documented diminished functional connectivity between the occipital lobule and basal ganglia in certain PD phenotypes, emphasizing the connection between visual processing and motor symptoms. In essence, PD progression doesn't only alter the DFC within the holistic brain network but also affects individual cortical subnetworks and the SN. This potentially elucidates the escalating spectrum of motor and non-motor symptoms in PD patients as the disease advances.

This study is not without limitations. Firstly, we did not include the longitudinal RS-fMRI data from healthy controls, limiting our ability to understand the impact of natural aging on longitudinal DFC changes. Secondly, it is well-established that dopaminergic medications affect RS-fMRI signals, as shown in FC,[26] DFC,[7] and network topology[2] studies. In the present study, due to limited data, we were unable to determine whether RS-fMRI acquisition and neurological functional assessments were performed during the medication-OFF. Thus, we can't ascertain the magnitude to which our results may have been influenced by the effects of dopaminergic medications. But the effect of dopaminergic medication may be present in two timepoints, therefore, there would have been a balancing effect on the data across timepoints. Thirdly, our sample size was relatively small, suggesting that a broader sample might produce more definitive results. Lastly, our study did not delve into PD's heterogeneity. Given that PD manifests differently among individuals, understanding these variations could provide deeper insights into its progression and impact.

In conclusion, our findings indicate that as PD advances, significant longitudinal shifts occur in the temporal aspects of DFC. Furthermore, these shifts

correlate directly with worsening neurological symptoms. This suggests that DFC holds promise as a valuable biomarker for assessing the progression of PD.

Values are presented as mean (SD). UPDRS = Unified Parkinson's Disease Rating Scale. ESS = Epworth Sleepiness Scale. GDS-SF = Geriatric Depression Scale Short Form. RBDSQ = REM Sleep Behavior Disorder Screening Questionnaire. MoCA = Montreal Cognitive Assessment.

REFERENCES

1. Allen, E.A., Damaraju E., Plis S.M., et al. (2014). Tracking whole-brain connectivity dynamics in the resting state. Cereb Cortex ***24,*** 663-676.
2. Berman, B.D., Smucny J., Wylie K.P., et al. (2016). Levodopa modulates small-world architecture of functional brain networks in parkinson's disease. Mov Disord ***31,*** 1676-1684.
3. Calabresi, P., Castrioto A., Di Filippo M., et al. (2013). New experimental and clinical links between the hippocampus and the dopaminergic system in parkinson's disease. Lancet Neurol ***12,*** 811-821.
4. Caminiti, S.P., Presotto L., Baroncini D., et al. (2017). Axonal damage and loss of connectivity in nigrostriatal and mesolimbic dopamine pathways in early parkinson's disease. Neuroimage Clin ***14,*** 734-740.
5. Campbell, M.C., Jackson J.J., Koller J.M., et al. (2020). Proteinopathy and longitudinal changes in functional connectivity networks in parkinson disease. Neurology ***94,*** e718-e728.
6. Yan,C.G.,and Zang, Y.F. (2010). Dparsf: A matlab toolbox for "pipeline" data analysis of resting-state fmri. Front Syst Neurosci ***4,*** 13.
7. Chen, L., Bedard P., Hallett M., et al. (2021). Dynamics of top-down control and motor networks in parkinson's disease. Mov Disord ***36,*** 916-926.
8. Cohen, J.R., and D'esposito M. (2016). The segregation and integration of distinct brain networks and their relationship to cognition. J Neurosci ***36,*** 12083–12094.
9. Cucca, A., Di Rocco A., Acosta I., et al. (2021). Art therapy for parkinson's disease. Parkinsonism Relat Disord ***84,*** 148-154.
10. Esteban, O., Markiewicz C.J., Blair R.W., et al. (2019). Fmriprep: A robust preprocessing pipeline for functional mri. Nat Methods ***16,*** 111-116.
11. Filippi, M., Basaia S., Sarasso E., et al. (2021). Longitudinal brain connectivity changes and clinical evolution in parkinson's disease. Mol Psychiatry ***26,*** 5429-5440.
12. Fiorenzato, E., Strafella A.P., Kim J., et al. (2019). Dynamic functional connectivity changes associated with dementia in parkinson's disease. Brain ***142,*** 2860-2872.
13. Guan, X., Zeng Q., Guo T., et al. (2017). Disrupted functional connectivity of basal ganglia across tremor-dominant and akinetic/rigid-dominant parkinson's disease. Front Aging Neurosci ***9,*** 360.
14. Gyorfi, O., Nagy H., Bokor M. et al. (2016). Behavioural aspects of a modified crosstalk between basal ganglia and limbic system in parkinson's disease. Neuropsychopharmacol Hung ***18,*** 87-92.
15. Helmich, R.C., Derikx L.C., Bakker M. et al. (2010). Spatial remapping of cortico-striatal connectivity in parkinson's disease. Cereb Cortex ***20,*** 1175-1186.
16. Hou, Y., Wei Q., Ou R. et al. (2021). Different resting-state network disruptions in newly diagnosed drug-naive parkinson's disease patients with mild cognitive impairment. BMC Neurol ***21,*** 327.
17. Hutchison, R.M., Womelsdorf T., Allen E.A., et al. (2013). Dynamic functional connectivity: Promise, issues, and interpretations. Neuroimage ***80,*** 360-378.
18. Kim, J., Criaud M., Cho S.S., et al. (2017). Abnormal intrinsic brain functional network dynamics in parkinson's disease. Brain ***140,*** 2955-2967.
19. Lewis, G.N., and Byblow W.D. (2002). Altered sensorimotor integration in parkinson's disease. Brain ***125,*** 2089–2099.
20. Li, W., Lao-Kaim N.P., Roussakis A.A., et al. (2020). Longitudinal functional connectivity changes related to dopaminergic decline in parkinson's disease. Neuroimage Clin ***28,*** 102409.
21. Liao, W., Wu G.R., Xu Q., et al. (2014). Dynamicbc: A matlab toolbox for dynamic brain connectome analysis. Brain Connect ***4,*** 780-790.
22. Nyberg, E.M., Tanabe J., Honce J.M., et al. (2015). Morphologic changes in the mesolimbic pathway in parkinson's disease motor subtypes. Parkinsonism Relat Disord ***21,*** 536-540.
23. Olde Dubbelink, K.T., Schoonheim M.M., Deijen J.B., et al. (2014). Functional connectivity and cognitive decline over 3 years in parkinson disease. Neurology ***83,*** 2046-2053.
24. Olde Dubbelink, K.T., Stoffers D., Deijen J.B., et al. (2013). Resting-state functional connectivity as a marker of disease progression in parkinson's disease: A longitudinal meg study. Neuroimage Clin ***2,*** 612-619.
25. Poewe, W., Seppi K., Tanner C.M., et al. (2017). Parkinson disease. Nat Rev Dis Primers ***3,*** 17013.
26. Powell, A., Muller A.J., O'callaghan C., et al. (2020). Dopamine and functional connectivity in patients with parkinson's disease and visual hallucinations. Mov Disord ***35,*** 704-705.
27. Schaefer, A., Kong R., Gordon E.M., et al. (2018). Local-global parcellation of the human cerebral cortex from intrinsic functional connectivity mri. Cereb Cortex ***28,*** 3095-3114.
28. Sharman, M., Valabregue R., Perlbarg V., et al. (2013). Parkinson's disease patients show reduced cortical-subcortical sensorimotor connectivity. Mov Disord ***28,*** 447-454.
29. Sveinbjornsdottir, S. (2016). The clinical symptoms of parkinson's disease. J Neurochem ***139 Suppl 1,*** 318-324.
30. Tessitore, A., Giordano A., De Micco R., et al. (2014). Sensorimotor connectivity in parkinson's disease: The role of functional neuroimaging. Front Neurol ***5,*** 180.
31. Tian, Y., Margulies D.S., Breakspear M., et al. (2020). Topographic organization of the human subcortex unveiled with functional connectivity gradients. Nat Neurosci ***23,*** 1421-1432.
32. Vossel, S., Geng J.J., and Fink G.R. (2014). Dorsal and ventral attention systems: Distinct neural circuits but collaborative roles. Neuroscientist ***20,*** 150–159.
33. Weil, R.S., Schrag A.E., Warren J.D. et al. (2016). Visual dysfunction in parkinson's disease. Brain ***139,*** 2827–2843.
34. Yan, C.G., Wang X.D., Zuo X.N., et al. (2016). Dpabi: Data processing & analysis for (resting-state) brain imaging. Neuroinformatics ***14,*** 339-351.
35. Yu, Q., Li Q., Fang W., et al. (2021). Disorganized resting-state functional connectivity between the dorsal attention network and intrinsic networks in parkinson's disease with freezing of gait. Eur J Neurosci ***54,*** 6633-6645.

ACKNOWLEDGMENTS

Data used in the preparation of this article were obtained from the PPMI database (www.ppmi-info.org/data). For up-to-date information on the study, visit www.ppmi-info.org. PPMI, a public private partnership, is funded by The Michael J. Fox Foundation. In addition, we would like to thank our participants for generously taking part in this research. This work was supported by grants from the Natural Science Foundation of China (81971070) and the National Key Research and Development Program of China (2022YFC2405100).

AUTHOR CONTRIBUTIONS

Fangang Meng, Yina Ma, Yang Li, designed research; Zhibao Li, Wei Chen, Xiaoyu Zeng, Jun Ni, Yuzhu Guo, performed research; Zhibao Li, Wei Chen, Xiaoyu Zeng, performed data analysis; Zhibao Li, Wei Chen, wrote the manuscript draft; Fangang Meng, Yina Ma, Yang Li, Hua Zhang, revised the manuscript draft.

DECLARATION OF INTERESTS

The authors declare no competing interests.

DATA AND MATERIALS AVAILABILITY

Data used in this Article are publicly available from the Parkinson's Progression Markers Initiative database (www.ppmi-info.org/data).

SUPPLEMENTAL INFORMATION

It can be found online at https://doi.org/10.59717/j.xinn-med.2023.100027

LEAD CONTACT WEBSITE

https://mylab.bnu.edu.cn/
https://shi.buaa.edu.cn/liyang

www.the-innovation.org/medicine

The Innovation Medicine, Volume *1*

Supplemental Information

Dynamic functional connectivity assesses the progression of Parkinson's disease

Zhibao Li, Wei Chen, Xiaoyu Zeng, Jun Ni, Yuzhu Guo, Hua Zhang, Yang Li, Yina Ma, and Fangang Meng

METHODS AND MATERIALS

Image preprocessing

Image data preprocessing was performed using DPABISurf, which is a surface-based RS-fMRI data analysis toolbox adapted from DPABI/DPARSF.[2, 16] The DPABISurf preprocesses the structural and functional MRI data using the fMRIprep pipeline.[5] We used several steps to process the MRI data: (1) the first 10 time points were removed for signal stabilization; (2) the image data were converted to BIDS format, and the fMRIprep 1.5.0 docker was called; (3) anatomical data preprocessing, which comprised the correction of T1-weighted (T1w) images for intensity non-uniformity using N4BiasFieldCorrection[15] (used as the T1w-reference image throughout the workflow), skull-stripping of the T1w-reference image using the Nipype implementation of the antsBrainExtraction workflow (from ANTs),[1] using OASIS30ANTs as the target template, segmentation of brain-extracted T1w brain tissue into cerebrospinal fluid (CSF), white matter (WM), and gray matter using FAST (from FSL 5.0.9),[17] and reconstruction of brain surfaces using recon-all (from FreeSurfer 6.0.1);[4] (4) fMRI data preprocessing, which comprised several preprocessing steps for each blood oxygen level-dependent (BOLD) runs per subject (across all tasks and sessions): a reference volume and its skull-stripped version were generated using a custom fMRIprep pipeline; susceptibility distortion correction was omitted; the BOLD reference image was co-registered to the T1w-reference image using bbregister (FreeSurfer), which implements boundary-based registration;[8] head-motion parameters with respect to the BOLD reference image (transformation matrices and six corresponding rotation and translation parameters) were estimated before spatiotemporal filtering using mcflirt (FSL 5.0.9);[12] BOLD runs were slice-time corrected using 3dTshift from AFNI 20160207;[3] BOLD time series were resampled into fsaverage5 space; (5) nuisance covariates regression, which included the Friston 24

parameter model,[6] mean framewise displacement (FD),[12] and linear regression, to remove the confounds of head motion, the residual effects of motion in group analyses, and other spurious variance (i.e., WM and CSF signals), and linear trends were entered as a regressor to account for drifts in the BOLD signal; (6) images were bandpass-filtered to 0.01–0.1 Hz and smoothed using a 6 mm full width at half maximum Gaussian kernel.

DFC Analysis with FLS

Please refer to previous studies[7, 9] for details about DFC analysis with flexible least squares (FSL). FSL was also conducted by the DynamicBC toolbox. FSL is a data-driven method which could yield frame-wise DFC, which means this approach can yield a DFC map at each time point for each scan. FLS uses a state-modeling based filtering approach and estimates a state (i.e., beta coefficient) by minimizing the errors associated with (1) discrepancies between the actual and estimated observation at each time point (measurement fit error), and (2) discrepancies due to incorrect specifications of the state transition equations (dynamic error). Two types of errors were characterized using ordinary least squares estimation. This is in contrary to static linear regression, where a single β coefficient is obtained by minimizing the residual fit error between two signals. The measurement fit error is given by

$$r_M^2(\beta, T) = \sum_{t=1}^{T} \big(y(t) - x(t)\beta(t)\big)^2, \#(1)$$

where x(t) and y(t) represent the values of two individual fMRI timeseries at time t, T is the total number of time points in the given timeseries, and β denotes the model fit coefficient vector. Dynamic error is given by

$$r_D^2(\beta, T) = \sum_{t=1}^{T-1} \big(\beta(t+1) - \beta(t)\big)^2, \#(2)$$

The errors in Equations (1) and (2) are combined into a single cost-incompatibility function weighted by a Lagrange multiplier μ, thus enabling multicriteria optimization. This function is minimized to estimate the β coefficient sequence, formally:

$$C(\beta, \mu, T) = \mu . r_D^2(\beta, T) + r_M^2(\beta, T), \#(3)$$

where μ denotes the weighting parameter (Lagrange multiplier) between the measurement fit error, r_M^2, and the dynamic error, r_D^2. The incompatibility cost function was minimized with ordinary least squares estimation, permitting the β(t) coefficients to vary over time. Therefore,

each FLS estimate (i.e., β(t) coefficient) shows the state vector evolved over time in a manner that minimizes the cost incompatibility function and maximizing the trueness of the priors defined in Equations (1) and (2). The weighting parameter μ arbitrates a trade-off between erratic solutions with large dynamic errors (i.e., small μ) and solutions that tend toward the static linear regression solution (i.e., large μ). Here, we used the default setting of $\mu = 100$ since this produced optimal variation in the β sequence.[13] This default setting is independent of the temporal resolution of fMRI acquisition (i.e., TR) and none of the equations governing FLS depend on the interval between time points. Furthermore, FLS is not limited by requirements of prior window length specifications associated with the commonly used sliding-window DFC, where an optimal choice of window length is arbitrary.[10, 11, 14, 18] For each individual, the frame-wise DFC computed by FSL would produce a 216 x 216 x 200 matrix of frame-wise DFC estimates.

Afterwards, we used k-means clustering algorithm to estimate reoccurring FC maps (state), which could be assessed by frequency and structure of these states. Please refer to the main text for the details of k-means cluster. To access the temporal properties of DFC, we calculate three various temporal indices: mean dwell time (MDT), fractional window (FW), and number of transitions (NT).

RESULTS

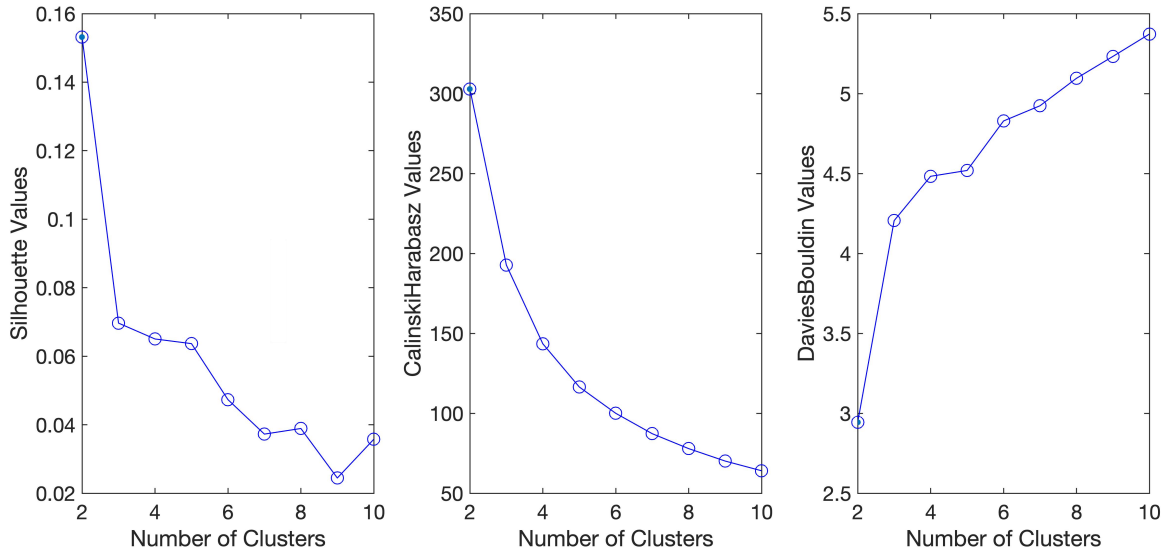

Figure S1 Estimating optimal clusters. The optimal clusters for all three criteria are 2.

The results of DFC analysis using sliding window approach with 416 ROIs. (Figure 2-4)

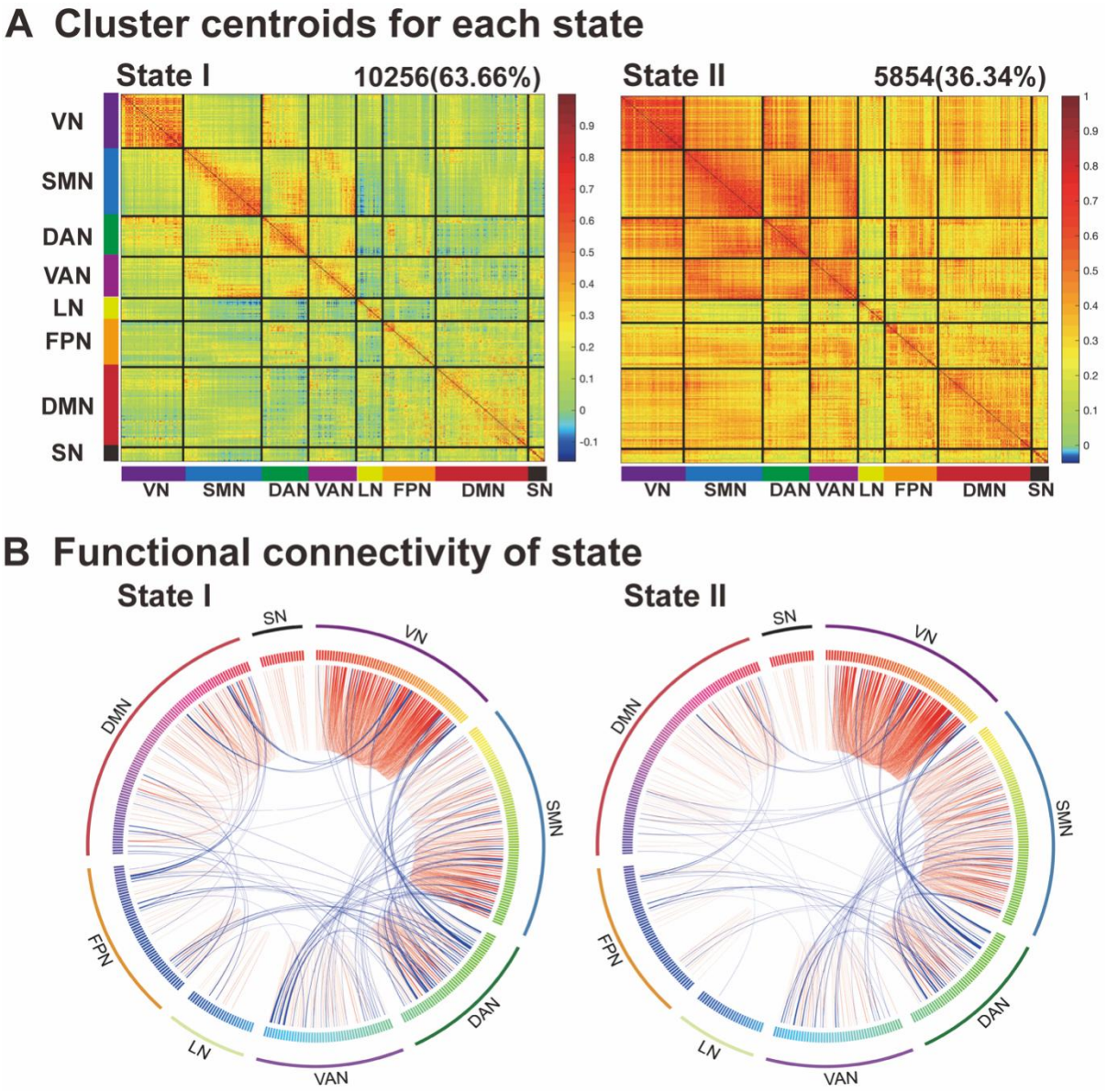

Figure S2. Results of the clustering analysis per state. (A) Cluster centroids for each state. The total number of occurrences and percentage of total occurrences are listed above each cluster median. (B) The chordal graph made by Circos shows only the top 1% of connections for each state. Red lines represent connections within-network, while blue lines depict connections between-networks.

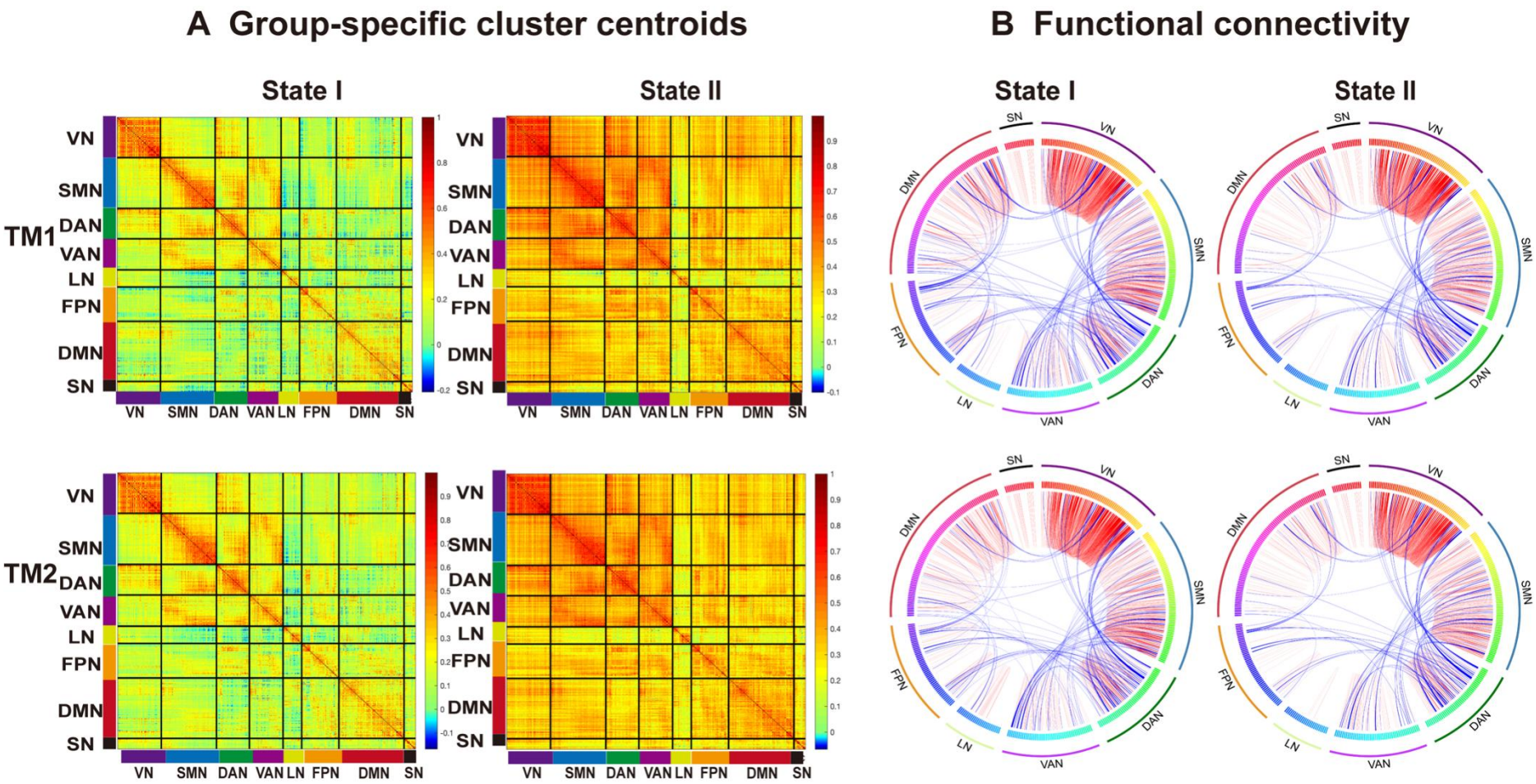

Figure S3. Functional connectivity state results. (A) timepoint-specific cluster centroid for each state. (B) The chordal graph made by Circos shows only the top 1% of connections for each state for timepoint I and timepoint II. Red lines represent connections within-network, while blue lines depict connections between-networks.

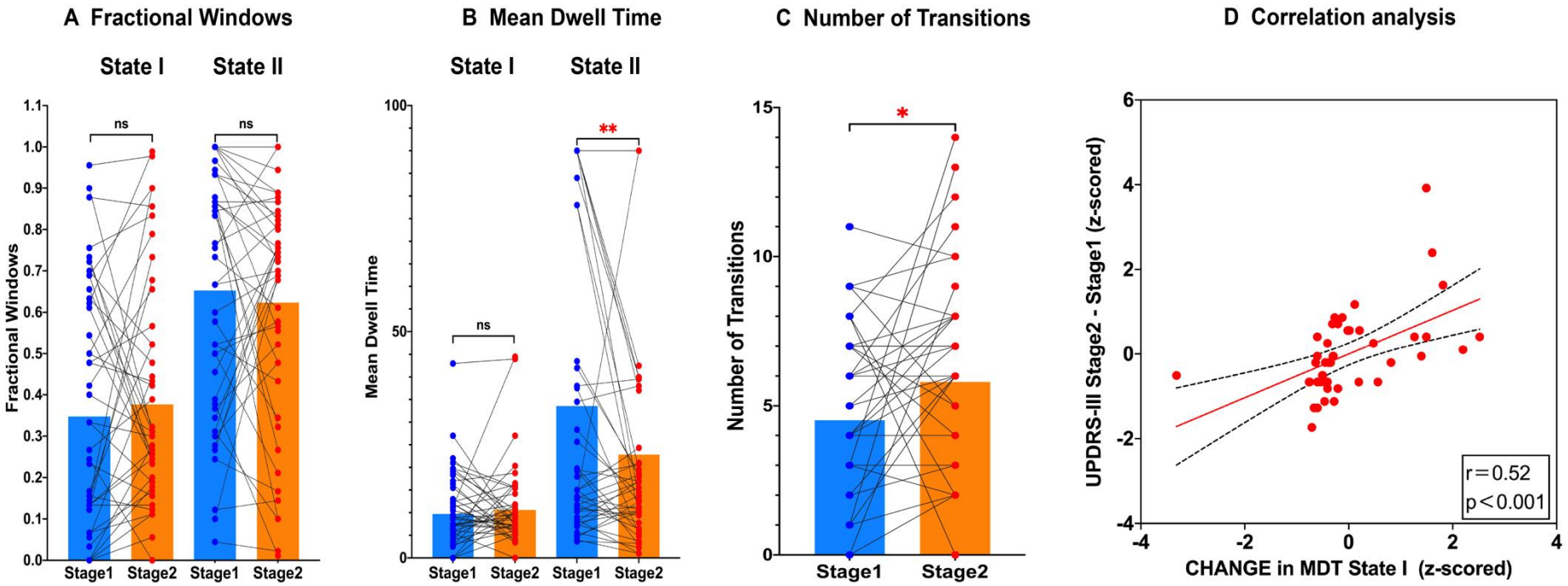

Figure S4. Results of between-timepoint comparisons of temporal properties of each FC state. (A) Results of between- timepoint comparisons of FW of each FC state. (B) Results of between- timepoint comparisons of MDT of each FC state. (C) Results of between- timepoint comparisons of TN of each FC state. (D) Results of correlation analysis between MDT changes (z-scored) in state I and motor attenuation (z-scored). (One asterisk indicates P<0.01, two asterisks indicate P<0.05, FDR corrected).

The results of DFC analysis using FSL approach with 216 ROIs. (Figure 5-7)

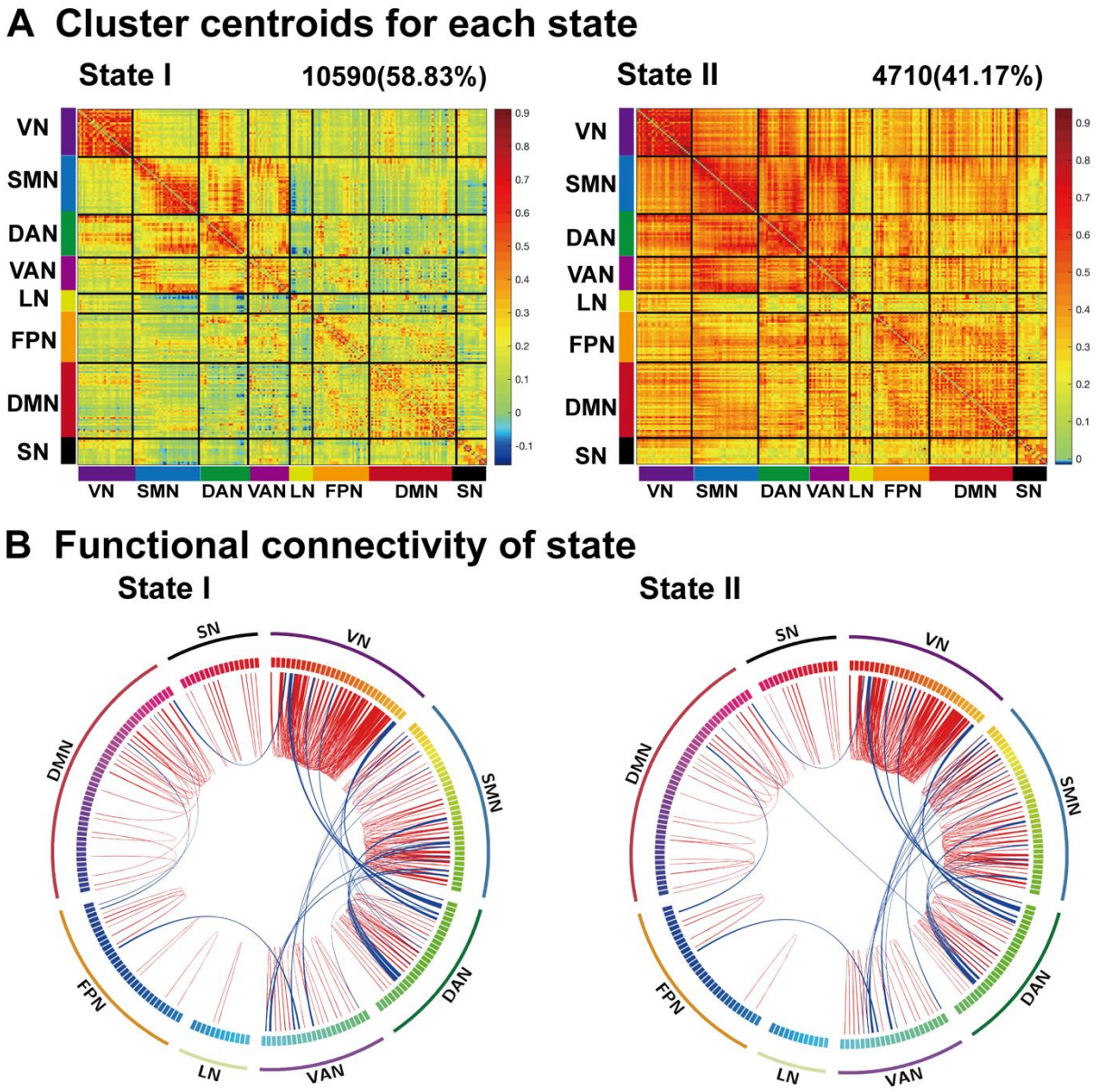

Figure S5. Results of the clustering analysis per state. (A) Cluster centroids for each state. The total number of occurrences and percentage of total occurrences are listed above each cluster median. (B) The chordal graph made by Circos shows only the top 1% of connections for each state. Red lines indicate intra-network connections, blue indicates inter-network connections.

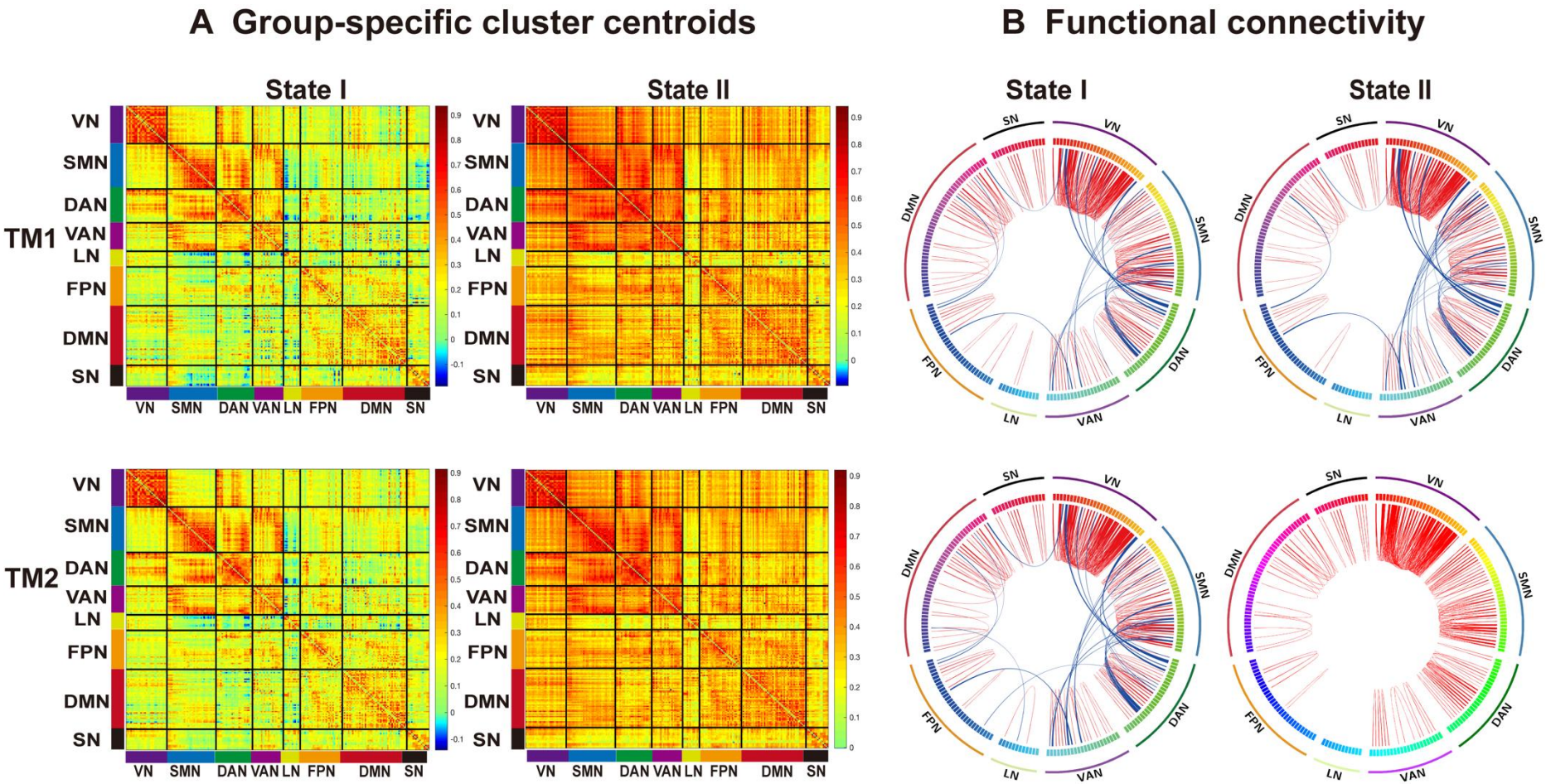

Figure S6. Functional connectivity state results. (A) Timepoint-specific cluster centroid for each state. (B) The chordal graph made by Circos shows only the top 1% of connections for each state for timepoint I and timepoint II. Red lines indicate intra-network connections, blue indicates inter-network connections.

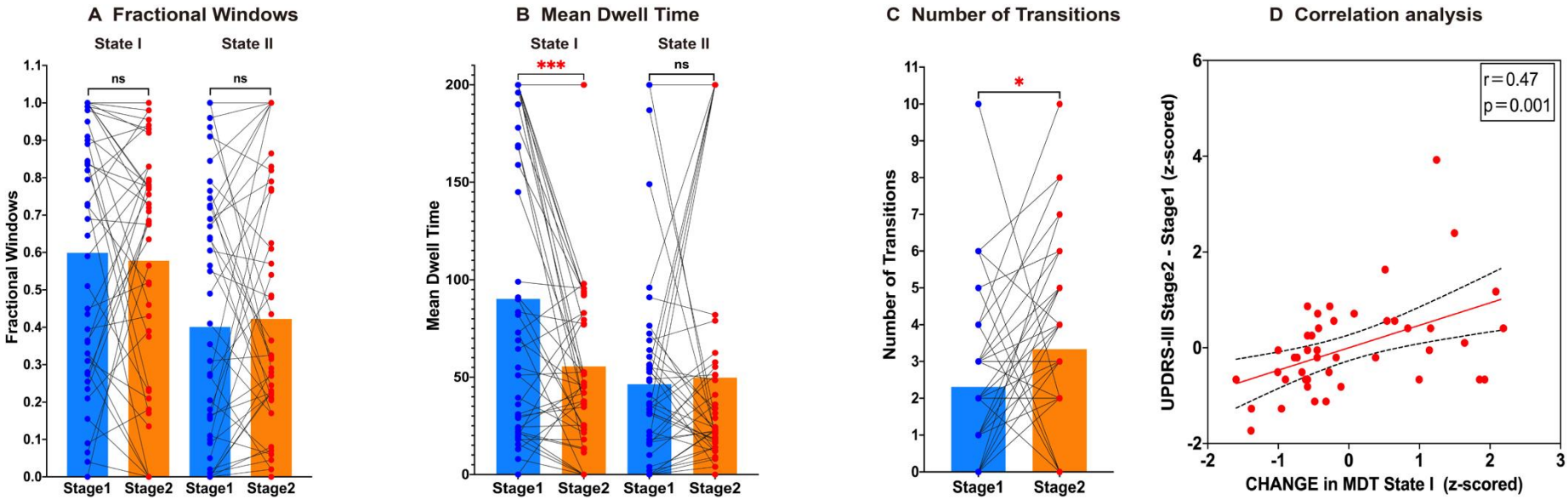

Figure S7. Results of between-timepoint comparisons of temporal properties of each FC state. (A) Results of between-timepoint comparisons of FW of each FC state. (B) Results of between-timepoint comparisons of MDT of each FC state. (C) Results of between-timepoint comparisons of TN of each FC state. (D) Results of correlation analysis between MDT changes (z-scored) in state I and motor attenuation (z-scored). (One asterisk indicates P<0.01, three asterisks indicate P<0.001, FDR corrected).

REFERENCE

1. Avants, B.B., Epstein C.L., Grossman M. *et al.* (2008). Symmetric diffeomorphic image registration with cross-correlation: Evaluating automated labeling of elderly and neurodegenerative brain. Med Image Anal ***12*****,** 26-41.
2. ChaoGan, Y., YuFeng Z. (2010). Dparsf: A matlab toolbox for "pipeline" data analysis of resting-state fmri. Front Syst Neurosci ***4*****,** 13.
3. Cox, R.W., Hyde J.S. (1997). Software tools for analysis and visualization of fmri data. NMR Biomed ***10*****,** 171-178.
4. Dale, A.M., Fischl B., Sereno M.I. (1999). Cortical surface-based analysis. I. Segmentation and surface reconstruction. Neuroimage ***9*****,** 179-194.
5. Esteban, O., Markiewicz C.J., Blair R.W. *et al.* (2019). Fmriprep: A robust preprocessing pipeline for functional mri. Nat Methods ***16*****,** 111-116.
6. Friston, K.J., Williams S., Howard R. *et al.* (1996). Movement-related effects in fmri time-series. Magn Reson Med ***35*****,** 346-355.
7. Ganesan, S., Lv J., Zalesky A. (2022). Multi-timepoint pattern analysis: Influence of personality and behavior on decoding context-dependent brain connectivity dynamics. Hum Brain Mapp ***43*****,** 1403-1418.
8. Greve, D.N., Fischl B. (2009). Accurate and robust brain image alignment using boundary-based registration. Neuroimage ***48*****,** 63-72.
9. Guo, X., Duan X., Suckling J. *et al.* (2019). Partially impaired functional connectivity states between right anterior insula and default mode network in autism spectrum disorder. Hum Brain Mapp ***40*****,** 1264-1275.
10. Hutchison, R.M., Womelsdorf T., Allen E.A. *et al.* (2013). Dynamic functional connectivity: Promise, issues, and interpretations. Neuroimage ***80*****,** 360-378.
11. Hutchison, R.M., Womelsdorf T., Gati J.S. *et al.* (2013). Resting-state networks show dynamic functional connectivity in awake humans and anesthetized macaques. Hum Brain Mapp ***34*****,** 2154-2177.
12. Jenkinson, M., Bannister P., Brady M. *et al.* (2002). Improved optimization for the robust and accurate linear registration and motion correction of brain images. Neuroimage ***17*****,** 825-841.
13. Liao, W., Wu G.R., Xu Q. *et al.* (2014). Dynamicbc: A matlab toolbox for dynamic brain connectome analysis. Brain Connect ***4*****,** 780-790.
14. Preti, M.G., Bolton T.A., Van De Ville D. (2017). The dynamic functional connectome: State-of-the-art and perspectives. Neuroimage ***160*****,** 41-54.
15. Tustison, N.J., Avants B.B., Cook P.A. *et al.* (2010). N4itk: Improved n3 bias correction. IEEE Trans Med Imaging ***29*****,** 1310-1320.
16. Yan, C.G., Wang X.D., Zuo X.N. *et al.* (2016). Dpabi: Data processing & analysis for (resting-state) brain imaging. Neuroinformatics ***14*****,** 339-351.
17. Zhang, Y., Brady M., Smith S. (2001). Segmentation of brain mr images through a hidden markov random field model and the expectation-maximization algorithm. IEEE Trans Med Imaging ***20*****,** 45-57.
18. Zhuang, X., Yang Z., Mishra V. *et al.* (2020). Single-scale time-dependent window-sizes in sliding-window dynamic functional connectivity analysis: A validation study. Neuroimage ***220*****,** 117111.